Mourad LOUCIF[1], Abdelkader MECHERNENE[1]

Laboratoire d'automatique de Tlemcen (LAT), Université de Tlemcen, Algeria (1)

doi:10.15199/48.2023.04.13

Maximum power point tracking for wind turbine with nonlinear direct powers control of DFIG integrated to grid using VOC

Abstract. *This paper is aimed to describe a wind energy conversion system, including a doubly fed induction generator (DFIG), a bidirectional converter in the rotor circuit the DFIG is able to work as a generator in both sub-synchronous and super-synchronous modes. The topology of a DFIG, stator is connected direct to the grid while the rotor is connected to grid with back to back converters. The wind turbine was controlled using a maximum power point tracking with linear PI regulator. The nonlinear backstepping controller is applied to the rotor side converter (RSC) for the independently control of active and reactive powers taking into consideration the full nonlinear model of the DFIG, we don't neglecting small stator resistor and using voltage oriented control (VOC). The grid side converter (GSC) is controlled by using the oriented voltage control strategy. Also the DC link voltage control ensures the operation of unity power factor by making the reactive power zero. The obtained results are very satisfactory for this new kind of application.*

Streszczenie. *Niniejsza praca ma na celu opisanie systemu konwersji energii wiatru, w sklad którego wchodzi dwustronnie zasilany generator indukcyjny (DFIG), dwukierunkowy przekształtnik w obwodzie wirnika, który DFIG może pracować jako generator zarówno w trybie podsynchronicznym, jak i nadsynchronicznym. Topologia DFIG, stojan jest podłaczony bezpośrednio do sieci, podczas gdy wirnik jest podączony do sieci za pomocą konwerterów typu back-to-back. Turbina wiatrowa była sterowana za pomocą śledzenia punktu mocy maksymalnej z liniowym regulatorem PI. Nieliniowy regulator krokowy zastosowano w przekształtniku po stronie wirnika (RSC) w celu niezależnego sterowania mocą czynną i bierną, biorąc pod uwagę pełny nieliniowy model DFIG, nie zaniedbując małego rezystora stojana i stosując sterowanie zorientowane na napięcie (VOC) . Konwerter po stronie sieci (GSC) jest sterowany za pomocą zorientowanej strategii sterowania napięciem. Również regulacja napięcia obwodu pośredniego zapewnia pracę z jednostkowym współczynnikiem mocy poprzez zerowanie mocy biernej. Uzyskane wyniki są bardzo zadowalające dla tego nowego rodzaju aplikacji.* ***(Śledzenie punktu mocy maksymalnej dla turbiny wiatrowej z nieliniową bezpośrednią kontrolą mocy DFIG zintegrowanego z siecią za pomocą VOC)***

Keywords: Wind turbine, MPPT, double fed induction generator, voltage oriented control, backstepping, grid side converter.
Słowa kluczowe: turbina wiatrowa, generator DFIG, maksymalna moc

Introduction

Renewable energy resources are revealed to be the serious alternatives to the polluting energies. There are many kinds of renewable energy resources, which are exploited all over the world like solar, geothermal, biomass, hydropower and wind. In the last decades, the installation of wind farms has been developed and received a great support from the most governments, thanks to their profitability and cleanliness [1].

A doubly fed induction generator (DFIG) is most commonly used in wind power generation. It is a wound rotor induction machine with slip rings attached at the rotor and fed by power converter. With DFIG, generation can be accomplished in variable speed ranging from sub-synchronous speed to super-synchronous speed. The power converters feeding the rotor winding is usually controlled in a current regulated PWM type, thus the stator current can be adjusted in magnitude and phase angle. The rotor side converter operates at the slip frequency and the power converter processes only the slip power. Thus if the DFIG is to be varied within $\pm$30% slip, the rating of the power converter is only about $\pm$30% of the rated power of the wind turbine. In this design the net power out of the machine is a summation of the power coming from the stator and the rotor [14]. Recently, with the rapid development of the power semiconductor devices, DFIG is an attractive choice for variable speed application such as the electrical machine drive and Renewable energy production.

The theory of field orientation control (FOC), commonly known as vector control was introduced by Hasse and Blaschke [3]. The standard method uses the stator flux orientation aligned with direct axis to control powers of double fed induction generator [1], [6], [10]. On the other hand, it has been proven that an alternative orientation can be used, namely the grid voltage oriented control (VOC). When VOC is adopted, obviously the system frame is aligned on the grid voltage, with main advantages the improved damping of these poles and an easy implementation [15], [17].

Nonlinear multivariable systems has been extensively studied in many books and papers, the design procedures for such high order nonlinear control systems may be complicated and vary from case to case [4], [5]. Therefore, under the control of nonlinear systems, the question of applicability is important and general method does not exist. All the efforts made in recent years aim to expand as much as possible, all of the systems that the method is applicable.

The Backstepping approach has been introduced in 1991 by Krstic, Kanellakopoulos and Kokotovic [2] and ensures overall stability control systems, usually multivariate and higher order. It is a method for synthesis of recursive class having triangular nonlinear systems form, regardless of their order.

Rotor side converter (RSC) and grid side converter (GSC), these two converters are based IGBT which provides the power flow in both directions from the grid to the rotor and the rotor to the grid, the GSC works a rectifier and the RSC a inverter in mode sub-synchronne therefore the power transits the grid to the rotor, in mode super-synchrone, the GSC works a inverter and the RSC a rectifier in this case the power fraction transits the rotor to the grid, the capacity of the voltage smoothing delivered by the rectifier is between the RSC and GSC for more details [21].

This paper is organized as follows: Section 2 is devoted to wind energy conversion system, which will be separately modeled: wind turbine, gearbox and DFIG in the $(d$-$q)$ rotating frame, a new modeling approach that uses active and reactive power as states. Section 3 show first, control of the wind turbine to get the maximum power point tracking using linear PI regulator, then the principle of voltage oriented control is presented to control stator powers using non linear backstepping controller applied to rotor side converter. Section 4 we adopt the grid side converter modeling, control and maintain the DC bus voltage constant with linear IP regulator and assure a unity power factor on the grid side in different conditions. Simulation tests and results are presented and discussed in section 5. Finally, Section 6 ends the paper with a conclusion.

System description and modeling

The system studied in the present paper is constituted of wind energy conversion system, which uses DFIG. The conversion chain can be divided into three interacting main components which will be separately modeled: wind turbine, gearbox, DFIG with the topology that stator is connected direct to the grid while the rotor is connected to grid with back to back converter as presented in Fig. 1.

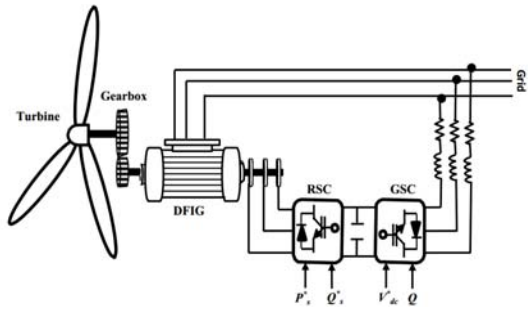

Fig. 1. Wind energy conversion system chain with DFIG

Wind turbine model

The expression for aerodynamic power and torque captured by the wind turbine are given by [6], [7]:

$$(1) \qquad \begin{cases} P_{aer} = \frac{1}{2} C_p(\lambda,\beta).\rho.\pi.R^2.V^3 \\ T_{aer} = C_p(\lambda,\beta).\frac{\rho}{2}.\pi.R^2.V^3 \frac{1}{\Omega_{turb}} \end{cases},$$

Where V is the wind speed, ρ is the air density, R is the blade radius and $Cp(\lambda,\beta)$ is the power coefficient which is a function of both λ tip speed ratio and β pitch angle which is described as [9]:

$$(2) \qquad \begin{cases} C_p = c_1 - c_2.(\beta - c_3).\sin(\lambda_i) - c_4.(\lambda - c_5).(\beta - c_6) \\ \lambda_i = \frac{\pi.(\lambda+0.1)}{14.8-0.3.(\beta-2)} \end{cases},$$

Table 1. Parameters coefficient value

c_1	c_2	c_3	c_4	c_5	c_5
0,5176	116	0.4	5	21	0.0068

The tip speed ratio is given by the following equation [8]:

$$(3) \qquad \lambda = \frac{\Omega_{turb}.R}{V},$$

$\Omega_{turb}$is the turbine rotational speed.

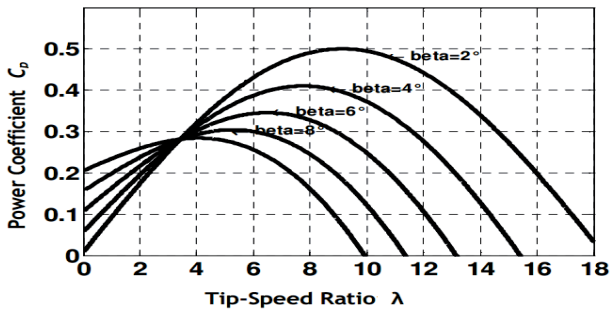

Fig. 2. Power coefficient versus tip-speed ratio for different values of the pitch angle

From Fig. 2, the maximum values of C_p is achieved for the curve associated to β = 2. From this curve, the maximum value of C_p (C_{pmax} = 0,5) and a particular value of λ is defined as the optimal value of tip speed ratio λ_{opt} = 9,15, which represents the optimum speed ratio. In These conditions we can apply the MPPT control.

Gearbox model

The expression of the gearbox G is given by [10]:

$$(4) \qquad T_g = \frac{T_{turb}}{G}, \ \ \Omega_{turb} = \frac{\Omega}{G},$$

Double fed induction generator model

The electrical equations of the DFIG in the synchronous frame are written as follow [11], [12]:

$$(5) \qquad \begin{cases} V_{sd} = R_s.i_{sd} + \frac{d\varphi_{sd}}{dt} - \omega_s.\varphi_{sq} \\ V_{sq} = R_s.i_{sq} + \frac{d\varphi_{sq}}{dt} + \omega_s.\varphi_s \\ V_{rd} = R_r.i_{rd} + \frac{d\varphi_{rd}}{dt} - (\omega_s - \omega).\varphi_{rq} \\ V_{rq} = R_r.i_{rq} + \frac{d\varphi_{rq}}{dt} + (\omega_s - \omega).\varphi_{rd} \end{cases},$$

Where R_s and R_r are the stator and rotor phase resistances, respectively. We note $\omega = p.\Omega$ the electrical speed and p is the number of pair poles.

The stator and rotor flux equations:

$$(6) \qquad \begin{cases} \varphi_{sd} = L_s.i_{sd} + M_{sr}.i_{rd} \\ \varphi_{sq} = L_s.i_{sq} + M_{sr}.i_{rq} \\ \varphi_{rd} = L_r.i_{rd} + M_{sr}.i_{sd} \\ \varphi_{rq} = L_r.i_{rq} + M_{sr}.i_{sq} \end{cases},$$

Where, L_s, L_r are respectively the stator and rotor inductances and M_{sr} is the magnetizing inductance. i_{sd}, i_{sq}, i_{rd} and i_{rq} are the direct and quadrature stator and rotor currents respectively.

The mathematical model of DFIG applied in the paper, has been obtained after the according to the voltage equations and equations of flux, expressed in a dq reference frame rotating at synchronous speed, the differential equations of the stator and rotor circuits of the generator with stator and rotor current as state variables can be given by [13], [14].

$$(7) \qquad \begin{cases} \frac{di_{sd}}{dt} = -a_1.i_{sd} + (a.\omega + \omega_s).i_{sq} + a_3.i_{rd} + a_5.\omega.i_{rq} \\ \quad + b_1.V_{sd} - b_3.V_{rd} \\ \frac{di_{sq}}{dt} = -(a.\omega + \omega_s).i_{sd} - a_1.i_{sq} - a_5.\omega.i_{rd} + a_3.i_{rq} \\ \quad + b_1.V_{sq} - b_3.V_{rq} \\ \frac{di_{rd}}{dt} = a_4.i_{sd} - a_5.\omega.i_{sq} - a_2.i_{rd} + \left(\omega_s - \frac{\omega}{\sigma}\right).i_{rq} \\ \quad - b_3.V_{sd} + b_2.V_{rd} \\ \frac{di_{rq}}{dt} = a_6.\omega.i_{sd} + a_4.i_{sq} - \left(\omega_s - \frac{\omega}{\sigma}\right).i_{rd} - a_2.i_{rq} \\ \quad - b_3.V_{sq} + b_2.V_{rq} \end{cases},$$

Where,

$$\sigma = 1 - \frac{M_{sr}^2}{L_s.L_r}, a = \frac{1-\sigma}{\sigma}, a_1 = \frac{R_s}{\sigma.L_s}, a_2 = \frac{R_r}{\sigma.L_r},$$

$$a_3 = \frac{R_r.M_{sr}}{\sigma.L_s.L_r}, a_4 = \frac{R_s.M_{sr}}{\sigma.L_s.L_r}, a_5 = \frac{M_{sr}}{\sigma.L_s}, a_6 = \frac{M_{sr}}{\sigma.L_r},$$

$$b_1 = \frac{1}{\sigma.L_s}, b_2 = \frac{1}{\sigma.L_r}, b_3 = \frac{M_{sr}}{\sigma.L_s.L_r}$$

The electromagnetic torque is expressed as:

$$(8) \qquad T_e = p\frac{M_{sr}}{L_s}\left(\varphi_{sq}.i_{rd} - \varphi_{sd}.i_{rq}\right),$$

The stator active and reactive powers are given as:

$$(9) \qquad \begin{cases} P_s = V_{sd}.i_{sd} + V_{sq}.i_{sq} \\ Q_s = V_{sq}.i_{sd} - V_{sd}.i_{sq} \end{cases},$$

Derivatives of stator active and reactive powers:

$$(10) \qquad \begin{cases} \dot{P}_s = V_{sd}.\frac{di_{sd}}{dt} + V_{sq}.\frac{di_{sq}}{dt} \\ \dot{Q}_s = V_{sq}.\frac{di_{sd}}{dt} - V_{sd}.\frac{di_{sq}}{dt} \end{cases},$$

Substituting (7) in (10), the derivatives stator active and reactive powers can then be expressed as follows:

(11)
$$\begin{cases} \dot{P}_s = -a_1.P_s - (\omega_s + a.\omega)Q_s + (a_5.\omega.V_{sd} + a_3.V_{sq})\, i_{rq} \\ +b_1.\left(V_{sd}^2 + V_{sq}^2\right) + (a_3.V_{sd} - a_5.\omega.V_{sq})\, i_{rd} \\ -b_3\left(V_{sd}.V_{rd} + V_{sq}.V_{rq}\right) \\ \dot{Q}_s = (\omega_s + a.\omega)P_s - a_1.Q_s + b_3\left(V_{sd}.V_{rq} - V_{sq}.V_{rd}\right) \\ + (a_5.\omega.V_{sd} + a_3.V_{sq})\, i_{rd} + (a_5.\omega.V_{sq} - a_3.V_{sd})\, i_{rq} \end{cases}$$

Wind turbine control

In order to capture the maximum power, we use the maximum power point tracking (MPPT) control with wind speed measurement developed in paper **[6]**.

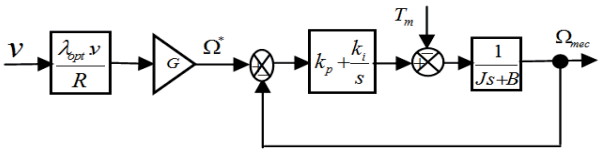

Fig. 3. Speed control loop using PI regulator

The turbine speed reference is expressed as:

(12)
$$\Omega_{turb}^{*} = \frac{\lambda_{opt}.V}{R},$$

(13)
$$\Omega^{*} = \Omega_{turb}^{*}.G,$$

The transfer function in closed loop can be determined as follows:

(14)
$$\frac{\Omega(s)}{\Omega_{ref}(s)} = \frac{\frac{k_i + k_p.s}{J}}{s^2 + \frac{k_p + B}{J}s + \frac{k_i}{J}}$$

The transfer function has a zero term in the numerator, identify the transfer function (14) with general second order defined by:

(15)
$$F(s) = \frac{2\xi\omega_n s + \omega_n^2}{s^2 + 2\xi\omega_n s + \omega_n^2},$$

allows determining the parameters proportional and integral gains:

(16)
$$\begin{cases} k_p = 2.\xi.\omega_n.J - B \\ k_i = J.\omega_n^2 \end{cases},$$

Where ξ is the damping coefficient (ξ =0.707) and ω_n is the undamped natural frequency.

Voltage oriented control

In the case studied, the proposed control a grid voltage orientated control (VOC) is adopted, in which the reference frame is chosen to align with the q-axis component of the stator voltage [15], [17], resulting as:

(17)
$$\begin{cases} V_{sd} = 0 \\ V_{sq} = V_s\,(cst) \end{cases},$$

Hence, the expressions of the derivatives stator active and reactive powers (11) are easily simplified as follow:

(18)
$$\begin{cases} \dot{P}_s = -a_1.P_s - (\omega_s + a.\omega)Q_s + a_3.V_s.i_{rq} + b_1.V_s^2 \\ \quad -a_5.\omega.V_s.i_{rd} - b_3.V_s.V_{rq} \\ \dot{Q}_s = (\omega_s + a.\omega)P_s - a_1.Q_s - b_3.V_s.V_{rd} + a_3.V_s.i_{rd} \\ \quad +a_5.\omega.V_s.i_{rq} \end{cases},$$

Backstepping control of rotor side converter

Backstepping control provides a systematic method to perform the design of a controller for nonlinear system. The idea is to computer a control law to ensure, for a positive definite Lyapunov function, the derivative time negative. The method is to divide the system into a set of nested subsystems descending. The calculation of the Lyapunov function is performed. Control is calculated in several steps and guarantees the overall system stability [18], [19].

The active and reactive power tracking errors e_1 and e_2 are defined respectively by:

(19)
$$\begin{cases} e_1 = P_s^{ref} - P_s \\ e_2 = Q_s^{ref} - Q_s \end{cases},$$

Where P_s^{ref} and Q_s^{ref} are the expected active and reactive powers references.

The derivative of equation errors variables gives:

(20)
$$\begin{cases} \dot{e}_1 = \dot{P}_s^{ref} - \dot{P}_s \\ \dot{e}_2 = \dot{Q}_s^{ref} - \dot{Q}_s \end{cases},$$

(21)
$$\begin{cases} \dot{e}_1 = \dot{P}_s^{ref} + a_1.P_s + (\omega_s + a.\omega)Q_s - b_1.V_s^2 \\ \quad -a_3.V_s.i_{rq} + b_3V_s.V_{rq} + a_5.\omega.V_s.i_{rd} \\ \dot{e}_2 = \dot{Q}_s^{ref} - (\omega_s + a.\omega)P_s + a_1.Q_s - a_5.V_s.i_{rd} \\ \quad +b_3.V_s.V_{rd} - a_5.\omega.V_s.i_{rq} \end{cases},$$

Choosing V as a Lyapunov function candidate:

(22)
$$\begin{cases} V(e_1) = \frac{1}{2}e_1^2 \\ V(e_2) = \frac{1}{2}e_2^2 \end{cases},$$

The derivative of equation errors variables gives:

(23)
$$\begin{cases} \dot{V}(e_1) = e_1.\dot{e}_1 = e_1.\left(\dot{P}_s^{ref} - \dot{P}_s\right) \\ \dot{V}(e_2) = e_2.\dot{e}_2 = e_2.\left(\dot{Q}_s^{ref} - \dot{Q}_s\right) \end{cases},$$

(24)
$$\begin{cases} \dot{V}(e_1) = e_1.\begin{pmatrix} \dot{P}_s^{ref} + a_1.P_s + (\omega_s + a.\omega)Q_s \\ -b_1.V_s^2 + b_3.V_s.V_{rq} + a_5.\omega.V_s.i_{rd} \\ -a_3.V_s.i_{rq} \end{pmatrix} \\ \dot{V}(e_2) = e_2.\begin{pmatrix} \dot{Q}_s^{ref} - (\omega_s + a.\omega)P_s + a_1.Q_s \\ +b_3.V_s.V_{rd} - a_5.V_s.i_{rd} - a_5.\omega.V_s i_{rq} \end{pmatrix} \end{cases},$$

The control algorithm proposed which is based on backstepping has been introduced:

(25)
$$\begin{cases} V_{rq} = \frac{1}{b_3.V_s}\begin{pmatrix} -\dot{P}_s^{ref} - a_1.P_s - (\omega_s + a.\omega)Q_s \\ +b_1.V_s^2 - a_5.\omega.V_s.i_{rd} + a_3.V_s.i_{rq} \\ -\lambda_1.e_1 \end{pmatrix} \\ V_{rd} = \frac{1}{b_3.V_s}\begin{pmatrix} -\dot{Q}_s^{ref} + (\omega_s + a.\omega)P_s - a_1.Q_s \\ +a_5.V_s.i_{rd} + a_5.\omega.V_s.i_{rq} - \lambda_2.e_2 \end{pmatrix} \end{cases},$$

With λ_1 and λ_2 are positives constants.

(26)
$$\begin{cases} \dot{V}(e_1) = e_1.\dot{e}_1 = -\lambda_1.e_1^2 \\ \dot{V}(e_2) = e_2.\dot{e}_2 = -\lambda_1.e_2^2 \end{cases},$$

Grid side converter modeling

Fig. 4 shows representation of the converter topology which is very similar to the machine side converter. L_g and R_g represent respectively the line resistance and inductance. i_{mdc} is the current out of the machine side converter, i_{gdc} is the current into the grid side inverter and i_{dc} is the current into the DC-bus capacitor; V_{gci} are the GSC output voltages.

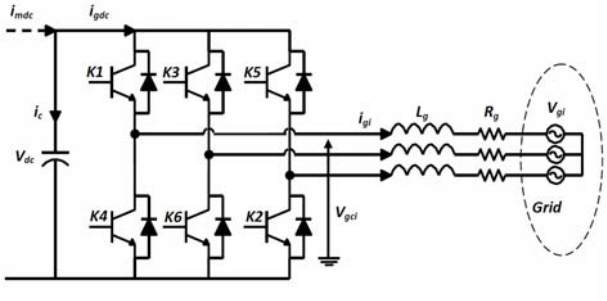

Fig. 4. Gid side converter

The grid phase voltages equations can be written as:

$$\begin{cases} V_{gca} = R_g.i_{ag} + L_g\frac{di_{ag}}{dt} + V_{ga} \\ V_{gcb} = R_g.i_{bg} + L_g\frac{di_{bg}}{dt} + v_{gb} \\ V_{gcb} = R_g.i_{cg} + L_g\frac{di_{cg}}{dt} + v_{gc} \end{cases}, \tag{27}$$

After Concordia and Park transformations, (27) can be expressed as follow, [21]:

$$\begin{cases} V_{gcd} = R_g i_{gd} + L_g\frac{di_{gd}}{dt} - \omega_s L_g i_{gq} + V_{gd} \\ V_{gcq} = R_g i_{gq} + L_g\frac{di_{gq}}{dt} + \omega_s L_g i_{gd} + v_{gq} \end{cases}, \tag{28}$$

Active and reactive powers, exchanged between the grid and the GSC, are given by the following equations:

$$\begin{cases} P_g = V_{gd} i_{gd} + V_{gq} i_{gq} \\ Q_g = V_{gq} i_{gd} - V_{dg} i_{gq} \end{cases}, \tag{29}$$

Grid side converter powers control

By using the oriented voltage control strategy, one can align the d-axis with the stator voltage, so:

$$V_{gq} = 0\,, \quad V_{gd} = V_d\,(cst), \tag{30}$$

Hence, the expressions of stator active and reactive powers (29), exchanged between the grid and the GSC, are easily simplified as follow:

$$\begin{cases} P_g = V_d\,.\,i_{gd} \\ Q_g = -V_d\,.\,i_{gq} \end{cases}, \tag{31}$$

Elsewhere, by neglecting the converter losses, the DC power has to be equal to the active power flowing between the grid and the GSC and one can write:

$$\begin{cases} V_{dc}\,.\,i_{dc} = V_d\,.\,i_{gd} \\ c\frac{V_{dc}}{dt} = i_{dc} - i_m \end{cases}, \tag{32}$$

From equation (32), we can note that the DC link voltage (V_{dc}) can be regulated by acting on the current i_{gd} in the voltage vector oriented reference frame. From equation (30), we can note also that the reactive power (Q_g) can be regulated to its reference value (Q_{gref}) by acting on the current i_{gq}. Consequently, to guarantee a unity power factor at the grid side, the reactive power command must be chosen as Q_{gref} = 0, so i_{qgref} = 0. Finally, after a dq-abc transformation of these reference currents (i_{gdref}, i_{gqref}), hysteresis modulation may then be used as shown in Fig. 5 [20].

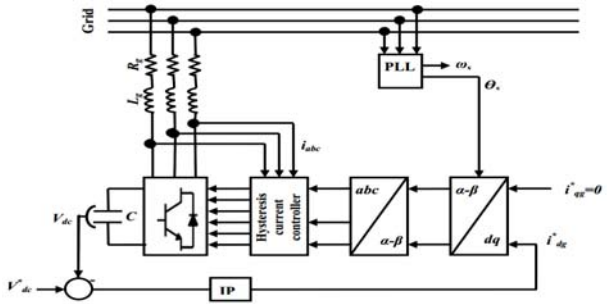

Fig. 5. Grid side converter powers control

DC bus voltage control

To improve the dynamic for transient state and avoid overshoots [22], the DC bus voltage control is confided to an integral and proportional (IP) controller. We can be represented by the block diagram shown in Fig. 6.

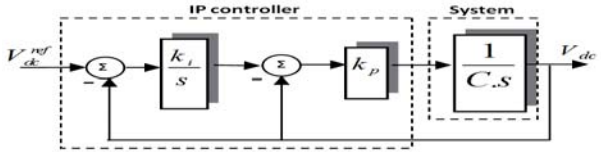

Fig. 6. DC link voltage control loop using IP controller

The transfer function in closed loop can be determined as follow

$$\frac{V_{dc}(s)}{\Omega^{ref}_{dc}(s)} = \frac{\frac{k_i.k_p}{C}}{s^2 + \frac{k_p}{C}s + \frac{k_p.k_i}{C}}, \tag{33}$$

The transfer function has no zero term in the numerator, identify the transfer function (32) with general second order defined by:

$$F(s) = \frac{2\xi\omega_n s + \omega_n^2}{s^2 + 2\xi\omega_n s + \omega_n^2}, \tag{34}$$

allows determining the parameters proportional and integral gains:

$$\begin{cases} 2\xi\omega_n = \frac{k_p}{C} \\ \omega_n^2 = \frac{k_p.k_i}{C} \end{cases}, \tag{35}$$

where

$$\begin{cases} k_p = 2.\xi.\omega_n.C \\ k_i = \frac{C.\omega_n^2}{k_p} \end{cases}, \tag{36}$$

Fig. 7 represent the application wind energy conversion system integrated to grid.

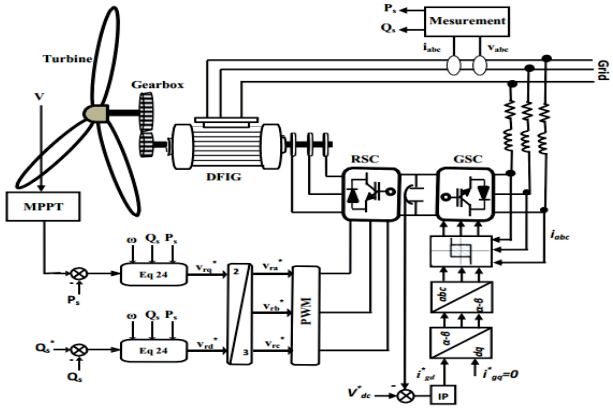

Fig. 7. Wind energy conversion system block diagram simulation

Simulation results

Simulation of the proposed strategies for the association of wind turbine with DFIG topology stator is connected direct to the grid while the rotor is connected to grid with back to back converters. The behavior analysis of the system for different operating conditions to verify the performance during the operation of sub-synchronous to super-synchronous generating modes. The wind turbine, DFIG and filter parameters are given in the appendix.

The model of the wind profile used in reference [23] is expressed by a summation of several harmonics in a deterministic form given by:

$$V = 8 + 0,2\sin(0,1047t) + 2\sin(0,2665t) + \sin(1,293t) + 0,2\sin(3,6645t) \tag{37}$$

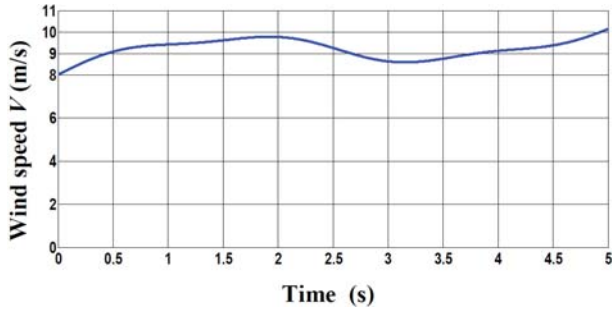

Fig. 8. Wind speed profile

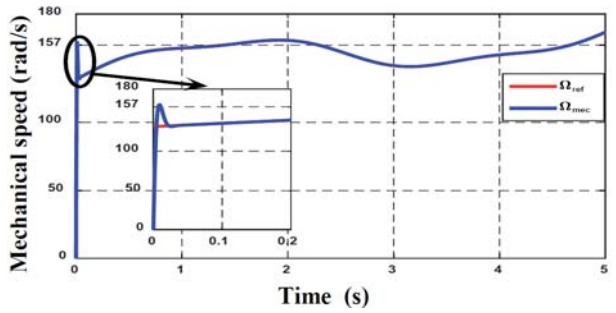

Fig. 9. Mechanical speed with MPPT

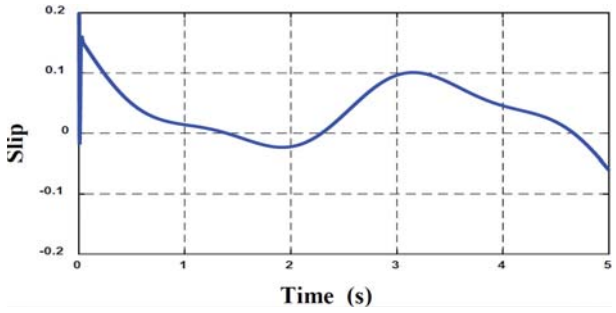

Fig. 10. The slip

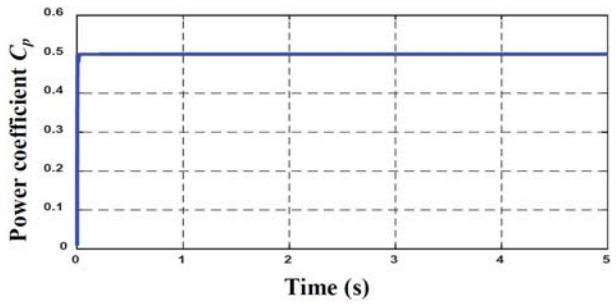

Fig. 11. Power coefficient

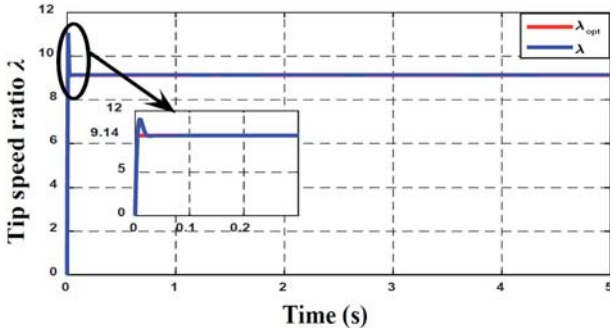

Fig. 12. Tip speed ratio

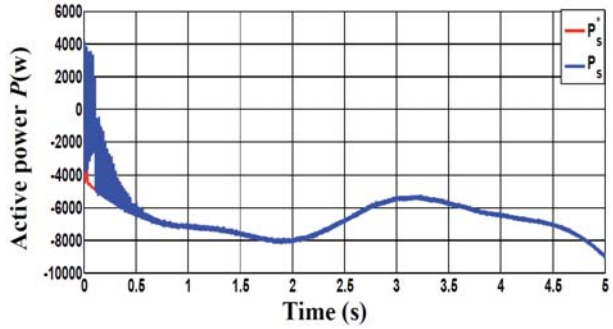

Fig. 13. Stator active power

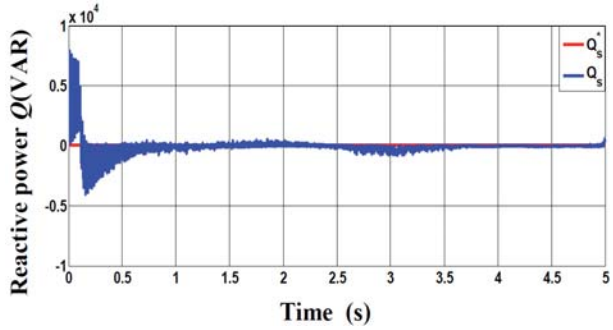

Fig. 14. Stator reactive power

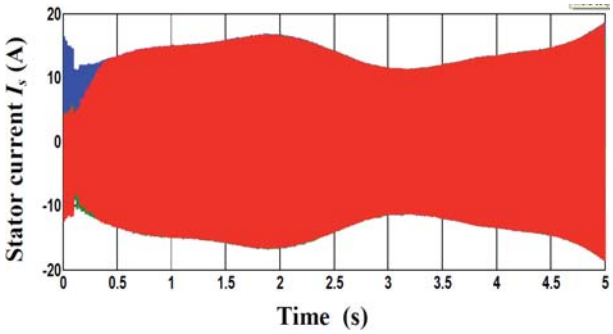

Fig. 15. Three phase stator current

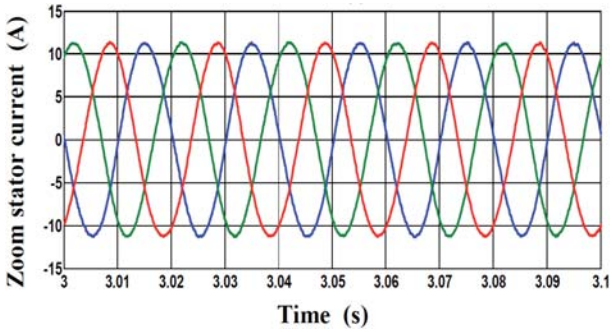

Fig. 16. Three phase stator current zoom

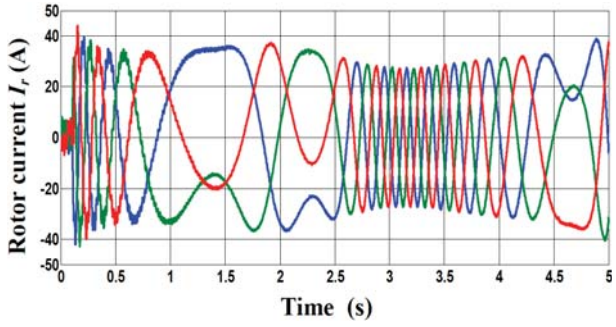

Fig. 17. Three phase rotor current

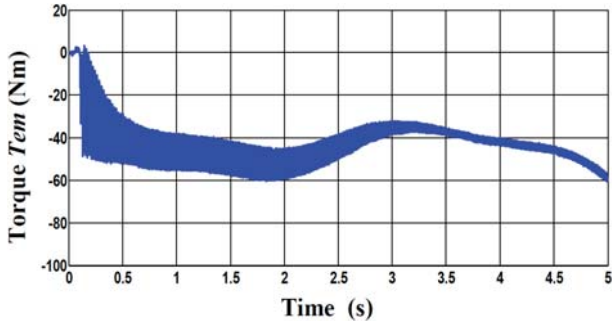

Fig. 18. Electromagnetic torque

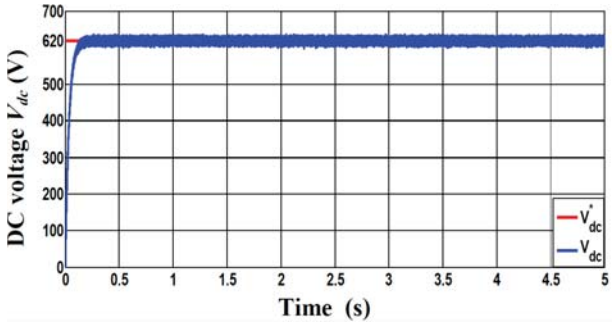

Fig. 19. DC link voltage

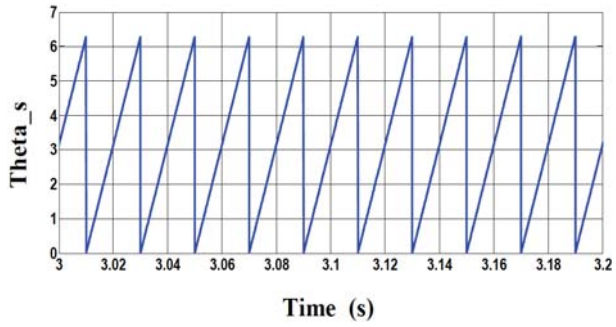

Fig. 20. Angular position stator using PLL

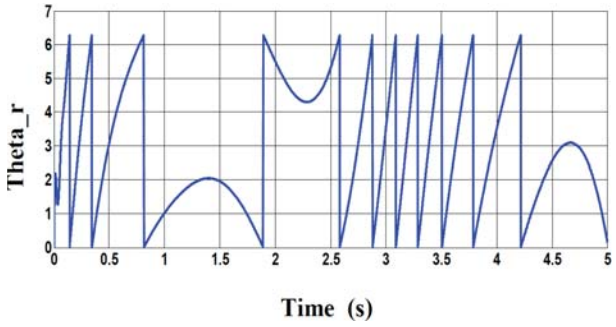

Fig. 21. Angular position rotor

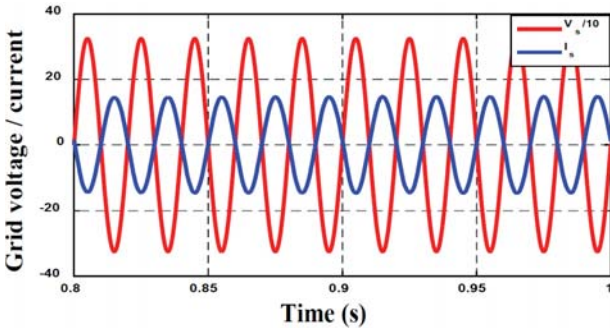

Fig. 22. Current and grid voltage

To extract the maximum power point tracking, for that a profile of the wind speed chosen in a manner to take into account the two operating processes in sub-synchronous and super-synchronous mode with an average speed of 8 m/s presented frome Fig. 8. In Fig. 9 shown the generator speed follows well the profile of the wind proposed, with a slight overshoot for a PI controller for maximum power point tracking (MPPT) in transient state, as well as it reference in steady state. The operation is sub-synchronous speed (<157 rad/s) and the slip is positive, then it is reaches for a speed of 9,5 m/s the operation is super synchronous speed (>157 rad/s) and the slip is negative, it is shown in Fig. 10. Fig. 11 present the evolution of power coefficient, it reache the optimal value (C_{pmax}=0,5) for pitch angle is chosen to be β =2. Fig. 12 show the optimal tip speed ratio (λ_{opt}=9,14), this can show that the tip speed ratio can follow the reference in steady state regime and a slight overshoot in transient regime.

In Fig. 13 the stator active power correctly follows almost perfectly its reference generated by the turbine with sign negative which means that the DFIG produces energy and delivered to the grid after the end of transient regime. The unit power factor is a guarantee for a reactive power of zero obtained after the end of its transient regime, as well as it reference in steady state regime is shown in Fig. 14. In Fig. 15 present the three phases stator currents are sinusoidal and constitute a balanced system of frequency 50Hz. It is very clear in the zoom of currents are sinusoidal and less disturbed is shown in Fig. 16. The three phases rotor currents are also sinusoidal, present a good tracking and the frequency of the current varies with the slip is shown in Fig. 17. The variation of the electromagnetic torque looks the same as that of the stator active power is shown in Fig. 18.

Adjusting the DC link voltage is shown in Fig. 19 with an IP controller give's a good track of the reference 620V without overshoot in transient regime, the static error is then null once the steady state reached. The angular position stator generated by the PLL is represented in Fig. 20. The angular position generated by the rotor is show the direction of the passage of the sub-synchronous to super synchronous modes operation in three zones of operation represented in Fig. 21. The grid current is in phase opposition with the generator voltage, Hence a unity power factor has been achieved it is very clear in Fig. 22.

Conclusion

This paper, present a modeling, control and simulation of the mechanical part of a wind turbine using a PI controller to extract the MPPT for the variable speed operating in region two is presented. It also presents the Backstepping controller of stator active and reactive powers control of a double fed induction generator using a stator voltage oriented applied to the rotor side converter. The second one is the DC bus voltage controller using IP regulator of the grid side converter, in two case studied sub-synchronous and super-synchronous operations. The results of simulation are presented and discussed confirming its feasibility of the proposed control scheme had a good follow regardless of variation wind speed profile.

Acknowledgement

This work is supported by the Direction Générale de la Recherche Scientifique et du Développement Technologique (DG RSDT), Algeria.

Appendix

Table 2. Wind turbine parameters

Parameters	**Value**	**Unite**
Nominal power P_n	10	Kw
Air density ρ	1,22	$Kg/^3$
Rotor radius R	3	m
Turbine inertia J_t	0,02	$Kg.m^2$
Turbine friction coefficient B_t	0,0016	$Nm/rad/s$
Number of blade	3	-
Gearbox ratio G	5,4	-

Table 3. DFIG parameters

Parameters	**Value**	**Unite**
Nominal power P_n	7,5	Kw
Nominal speed N_n	1440	Rpm
Number of poles pair p	2	-
Stator resistance R_s	0.455	Ω
Rotor resistance R_r	0.62	Ω
Stator inductance L_s	0,084	mH
Rotor inductance L_r	0,081	mH
Stator-rotor mutual inductance M_sr	2,691.10^5	mH
Moment of inertia J	0,3125	$N.m.s^2$
Coefficient of friction B	6.73e-3	$kg.m/s$

Table 4. Filter RL and the DC bus

Parameters	**Value**	**Unite**
Filter resistance R_g	0.4	Ω
Filter inductance L_g	4	mH
Capacitor C	2e^{-3}	F

***Authors**: Mourad Loucif, Laboratoire d'automatique de Tlemcen (LAT), Department of Electrical and Electronics Engineering, Faculty of Technology, University Abou Bekr Belkaid, Chetouane B.P 230 Tlemcen, Algeria*
email: loucif_mourad@live.fr
Abdelkader Mechernene, Laboratoire d'automatique de Tlemcen (LAT), Department of Electrical and Electronics Engineering, Faculty of Technology, University Abou Bekr Belkaid, Chetouane B.P 230 Tlemcen, Algeria
email: mechernene_aek@hotmail.com

REFERENCES

[1] Yessef M., Bossoufi B., Taoussi M., Lagrioui A., Chojaa H.,: Improved hybrid control strategy of the doubly-fed induction generator under a realwind profile, International Conference Digital Technologies and Applications, pp. 1724–1735, 2021.

[2] Krstic M., Kanellakopoulos I., Kokotovic P.V.,: Nonlinear and Adaptive Control Design, Wiley, New York, 1995.

[3] Blaschke F.: The principle of field oriented as applied to the new transvector closed-loop control system for rotating-field machine, Siemens Review XXXIX, 5(4), pp. 217-220, 1972.

[4] Utkin V.I.: Variable Structure Systems with Sliding Mode, IEEE. Trans. Automatic Control, 22(2), pp. 212-222

[5] Gille J.C.: Systs asservis non linaires, Edition Dunod

[6] Loucif M., Boumediene A., Mechernene A.: Maximum power point tracking based on backstepping control of wind turbine, Electrotehnica, Electronica, Automatica, (EEA), 62(3), Sep. 2014.

[7] Doumi M., Aissaoui A., Tahour A., Abid M., Thir K.: Nonlinear integral backstepping control of wind energy conversion system based on a double-fed induction generator, Przeglad Elektrotechniczny, 92(3), 2016.

[8] Loucif M., Boumediene A.: Modeling and direct power control for a DFIG under wind speed variation, Proceedings of the 3rd international conference on control, engineering information technology, Tlemcen, Algeria. May. 2015.

[9] El Aimani S.: Modélisation de différentes technologies d'éoliennes intégrées dans un réseau de moyenne tension, PHD thesis Doctorat, Lille, 2004.

[10] Ayrir W., Ourahou M., Haddi A.: DFIG stator reactive and active power control based fuzzy logic, International journal of circuits, systems and signal processing, 12, 2018.

[11] Mohammedi M., Bendiabdellah A., Allaoui T., Cherif B.: Wind energy conversion system control robustness based on current analysis of IGBT open-circuit fault, Przeglad Elektrotechniczny, 96(10), 2020.

[12] Bossoufi B., Karim M., Lagrioui A., Taoussi M., Derouich A.: Observer backstepping control of DFIG generators for wind turbines variable speed: FPGA based implementation, Renewable Energy Journal, 81, pp. 903–917, 2015.

[13] Lihui Y., Xikui M., Dong D.: Hopf bifurcation in doubly fed induction generator under vector control, Chaos, Solitons Fractals, 2009.

[14] Loucif M.: Synthèse de lois de commande non-linéaires pour le contrôle d'une machine asynchrone á double alimentation dédiée áun système aérogénérateur, PHD Thesis Doctorat, University of Tlemcen, 2016.

[15] Bourdoulis M., Alexandridis A.: A new controller design and analysis of dfig wind turbine systems for mpp operation, EuroCon. Zagreb, Croatia, 2013.

[16] Loucif M., Mechernene A.: Integral backstepping power control of DFIG based nonlinear modeling using voltage oriented control, International Conference Digital Technologies and Applications, pp. 1724–1735, 2021.

[17] Bourdoulis M., Alexandridis A.: Nonlinear stability analysis of dfig wind generators in voltage oriented control operation, European Control Conference (ECC), Zrich, Swit-zerland, 2013.

[18] El Mourabit Y., Derouich A., El Ghzizal A., El Ouanjli N., Zamzoum O.: Nonlinear backstepping control for PMSG wind turbine used on the real wind profile of the Dakhla-Morocco city, Int Trans Electr Energ Syst, 2020.

[19] Loucif M., Boumediene A., Mechernene A.: Backstepping control of double fed induction generator driven by wind turbine, Proceedings of the 3rd International Conference on Systems and Control, Algiers, Algeria, October. 2013.

[20] Loucif M., Boumediene A., Mechernene A.: Nonlinear sliding mode power control of DFIG under wind speed variation and grid connexion, Electrotehnica, Electronica, Automatica, (EEA), 63(3), Sep. 2015.

[21] Riouch T., El bachtiri R.: Robust control of the active and reactive power exchanged with the rotor of the DFIG and the grid, WSEAS transactions on environment and development, 9(1), 2013.

[22] Mechernene A., Zerikat M., Chekroun S.: Dynamical performances of sensorless vector control induction motor drive with a new adaptive neural network speed observer, Sciences and Techniques of Automatic Control, 2010.

[23] Abdenour Abdelli.: Optimisation multicrit d'une cha ienne passive, PHD thesis of the national polytechnic institute of Toulouse., Plasma and energy conversion laboratory, 2007.